catalysts

MDPI

Article

Engineering of a Novel, Magnetic, Bi-Functional, Enzymatic Nanobiocatalyst for the Highly Efficient Synthesis of Enantiopure (R)-3-Quinuclidinol

Qingman Li [1,†], Qihua Jiang [2,†], Pengcheng Gu [3], Lianju Ma [3,*] and Yiwu Wang [3,*]

[1] The First Clinical College, Chongqing Medical University, Chongqing 400016, China; lqm5858@163.com
[2] Department of Medicinal Chemistry, School of Pharmacy, Chongqing Medical University, Chongqing 400016, China; 100877@cqmu.edu.cn
[3] Lab Teaching & Management Center of Chongqing Medical University, Chongqing 400016, China; gupengcheng@cqmu.edu.cn
* Correspondence: malianjucq@126.com (L.M.); willwyw@cqmu.edu.cn (Y.W.); Tel.: +86-23-6848-5161 (L.M. & Y.W.); Fax: +86-23-6571-3519 (L.M. & Y.W.)
† Qingman Li and Qihua Jiang contributed equally to this work.

Abstract: Ni^{2+}-NTA-boosted magnetic porous silica nanoparticles (Ni@MSN) to serve as ideal support for bi-functional enzyme were fabricated for the first time. The versatility of this support was validated by one-step purification and immobilization of bi-functional enzyme MLG consisting of 3-Quinuclidinone reductase and glucose dehydrogenase, which can simultaneously catalyze both carbonyl reduction and cofactor regeneration, to fabricate an artificial bi-functional nanobiocatalyst (namely, MLG-Ni@MSN). The enzyme loading of 71.7 mg/g support and 92.7% immobilization efficiency were obtained. Moreover, the immobilized MLG showed wider pH and temperature tolerance and greater storage stability than free MLG under the same conditions. The nanosystem was employed as biocatalyst to accomplish the 3-quinuclidinone (70 g/L) to (R)-3-quinuclidinol biotransformation in 100% conversion yield with >99% selectivity within 6 h and simultaneous cofactor regeneration. Furthermore, the immobilized MLG retained up to 80.3% (carbonyl reduction) and 78.0% (cofactor regeneration) of the initial activity after being recycled eight times. In addition, the MLG-Ni@MSN system exhibited almost no enzyme leaching during biotransformation and recycling. Therefore, we have reason to believe that the Ni@MSN support gave great promise for constructing a new biocatalytic nanosystem with multifunctional enzymes to achieve some other complex bioconversions.

Keywords: porous silica nanoparticles; immobilized enzyme; nanosystem; cofactor regeneration; (R)-3-quinuclidinol; biocatalysts' recycling

Citation: Li, Q.; Jiang, Q.; Gu, P.; Ma, L.; Wang, Y. Engineering of a Novel, Magnetic, Bi-Functional, Enzymatic Nanobiocatalyst for the Highly Efficient Synthesis of Enantiopure (R)-3-Quinuclidinol. *Catalysts* **2021**, *11*, 1126. https://doi.org/10.3390/catal11091126

Academic Editor: Evangelos Topakas

Received: 17 August 2021
Accepted: 16 September 2021
Published: 18 September 2021

1. Introduction

Nanoparticles are widely applied in biomedical and industrial fields due to their unique features such as their porous nature and high surface area [1]. Enzymes, which are well-known, excellent performers and highly selective biocatalysts, therefore, have attracted significant attention in many areas such as the pharmacy industry, industrial synthesis, and environmental protection. Although promising, the use of pure enzymes in practical applications is hindered by their fragile nature, high cost for purification, low recyclability, and poor operational stability [1,2]. Enzyme immobilization is a promising strategy to overcome these disadvantages and concurrently improve the enzyme activity and stability [1,3–6]. To date, immobilization strategy mainly involves the formation of cross-linked enzyme aggregates (CLEAs), encapsulating an enzyme in a matrix by physical absorption, or covalently binding an enzyme to a solid support [6–9]. For CLEAs, although there is the appeal of a carrier-free immobilization method, optimization of the cross-linking procedure is time consuming, costly, and has poor mechanical resistance [7,8].

The immobilized enzyme by the physical absorptions generally is too weak to prevent the enzyme leaking from the support; therefore, additional covalent binding is often required [6–8]. Similarly, covalently bonding an enzyme to the support also has the drawback that, if the enzyme is irreversibly deactivated, the enzyme as well as the support are rendered useless [6,8]. Therefore, numerous supports such as polymeric, metallic, colloidal, non-porous materials have been developed to immobilize wide ranges of enzymes, thus improving enzymatic performance [3,9–11]. However, many shortcomings are associated with these supports, e.g., low enzyme loading in the non-porous systems and denaturation of enzyme in sol-gels due to their brittle and disordered structures [10,12]. Fortunately, extensive research efforts have revealed that porous support is an attractive candidate for enzyme immobilization due to chemical and thermal stability, large surface areas, and tunable pore structures capable of entrapping various enzymes within them, which afford a more stable environment compared with that of a planar surface [3,9,11]. However, the enzyme immobilized onto porous support in many cases exhibits reduced activity compared with those of the free enzyme and cannot be efficiently recycled due to the enzyme leaching during multiple reuses. Additionally, surface charges and aggregation inside the channel may promote enzyme denaturation or reduce the enzyme loading, thus hampering the conventional porous support used for enzyme immobilization [3,10,12]. By comparison, metal organic frameworks (MOFs) are unique, which are regarded to be an ideal porous network to immobilize the enzyme for biocatalytic applications [3,13–18]. However, there are cases in which it takes several days to engender MOFs' formation, and the weak non-covalent interactions between enzymes with MOFs are vulnerable to significant enzyme leaching. Thus, the search for more efficient immobilization systems to give high loading as well as efficiency is highly desirable.

Several extensively utilized methods of increasing importance in molecular biology are based on the ability of the immobilized Ni^{2+} by a chelating group, such as nitrilotriacetic acid (NTA) covalently bound to a solid support, to selectively bind His_6-tagged enzymes (namely, immobilized metal iron affinity chromatography, IMAC), making it possible to selectively purify and immobilize His_6-tagged enzymes. Notably, the IMAC-based immobilization method can maintain enzyme conformation, reduce the possibility of enzyme denaturation [19], and minimize enzyme leaking due to the strong coordination interactions (10^{-13} M) [20]. Therefore, the immobilized enzyme could be directly used as a biocatalyst for various biotransformations. For example, a highly active and recyclable biocatalyst consisting of Ni-NTA-modified magnetic nanoparticles was developed for enantioselective hydrolysis of racemic 2-(4-chlorophenyl)oxirane [21] and biotransformation of waste grease to biodiesel [22] and O-acetyl-L-serine to β-pyrazol-1-yl-L-alanine [23]. Notably, negligible losses of enzyme (only 0.02%) were released after each cycle [21]. Similarly, porous silica nanoparticles containing Ni-NTA groups on the surfaces have been reported to immobilize organophosphohydrolase for biodegradation of organophosphorus pesticides [24], or DNase, coagulase, and α-amylase against Gram-positive and -negative bacteria [25]. More importantly, the immobilization based on Ni-NTA-functionalized magnetic or porous silica nanoparticles can overcome some limitations of IMAC such as poor mechanical stability, limited surface area of agarose bead accessible for binding, etc. [24].

The (R)-3-quinuclidinol is widely used to synthesize aclidinium bromide [26], revatropate [27], solifenacin [28], etc. Advancements in biocatalysis' techniques have strongly boosted its recognition as a promising alternative for outpacing the inherent constraints of chemical synthesis such as being environmentally unfriendly and the production of many byproducts. Therefore, significant effort has been devoted to developing an efficient biocatalyst for(R)-3-quinuclidinol synthesis. Despite the high selectivity, whether wide-type [29,30] or engineered microorganism [31,32] whole cell as biocatalyst, it is difficult to recycle and reuse. Moreover, most of them proceed at low substrate loading, even only 2 g/L, and/or need a long bioconversion period, and/or need addition of external cofactor. Recently, Chen et al. created a bi-functional enzyme MLG consisting of M*l*QR (3-Quinuclidinone Reductase from Microbacterium luteolum) and GDH (glucose

dehydrogenase from Bacillus megaterium), which exhibited high catalytic activities for (R)-3-quinuclidinol synthesis and cofactor regeneration of great capacity, leading to much better substrate tolerance and 20-fold increase in the bioconversion rate over the parent enzymes [33]. Even so, there are still much room for improvement such as being unable to recycle and reuse, problems such as the mass transfer of substrates across cell membranes, etc.

To the best of our knowledge, using the bi-functional enzyme immobilized by affinity interaction onto an integrated supermagnetic porous silica support with further functionalization through grafting NTA for chelating Ni^{2+} as cofactor self-sufficient heterogeneous biocatalyst for asymmetric syntheses has not been reported to date. Herein, we present a novel Ni^{2+}-NTA-boosted, magnetic, porous, silica nanoparticle (Ni@MSN) capable of one-pot purifying and immobilizing the bi-functional enzyme MLG from cell lysates to fabricate an artificial bi-functional nanobiocatalyst (MLG-Ni@MSN), which exhibited improved environment tolerance, storage stability, and catalytic activity. The artificial biocatalytic nanosystem was employed as a biocatalyst to accomplish (R)-3-quinuclidinol bioconversion without supplying an external cofactor, easily recovered from the reaction medium and exhibiting a commendable reusability, subsequently resulting in greatly reducing the cost of the process. The sketch map of enzyme immobilization, reusability, and recycling of the biocatalyst and reuse of support is proposed in Scheme 1.

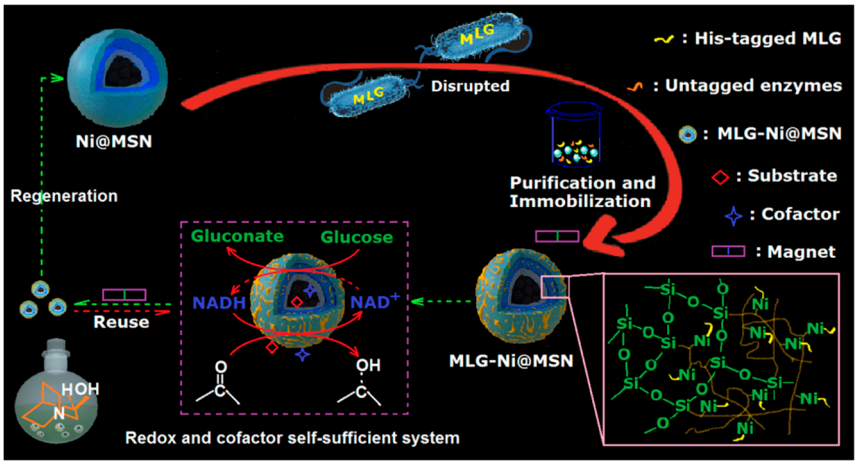

Scheme 1. Schematic description of one-pot purification and immobilization of bi-functional enzyme MLG onto Ni@MSN support followed by application in (R)-3-quinuclidinol synthesis, and subsequently recycling and reusing the biocatalyst.

2. Results and Discussion

2.1. Synthesis of Ni@MSN Support

Ni@MSN support was synthesized by the synthetic route, as shown in Scheme 2. Stepwise chemical modification first involved grafting TEOS onto the surface of Fe_3O_4 nanoparticles and subsequently coupling MPS to afford MSN with -C=C- bond, which can produce covalent bonds between the inorganic substrate and NTA-monomer [34]. For NTA-monomer synthesis, starting from N,N-bis(carboxymethyl)-L-lysine, the nucleophilic substitution proceeded with an excess of acryloychloride in the presence of NaOH to obtain the desired product with -C=C- bond. Afterwards, polymerization of NTA-monomer with MSN in the presence of MBA as cross-linker afforded the core-shell NTA-functionalized MSN. Finally, Ni^{2+} was loaded onto the NTA arms, obtaining Ni@MSN support, which was more stable than the Ni-NTA-MNPs coupled NTA by Schiff base [21,22,24].

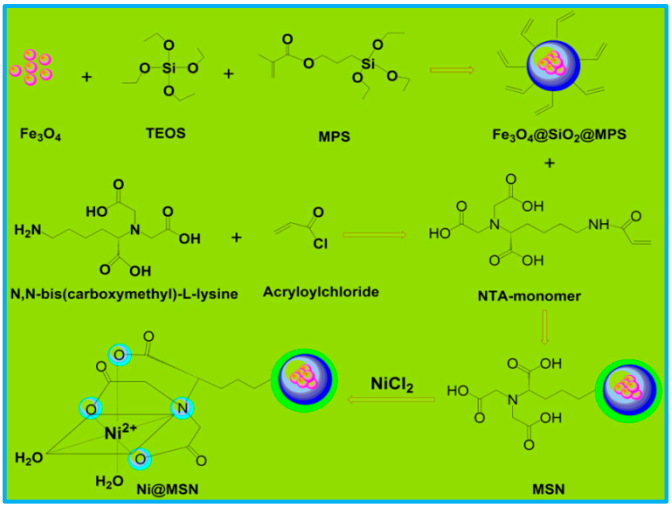

Scheme 2. Route for synthesis of NTA-monomer and Ni@MSN support.

2.2. Expression of Bi-Functional Enzyme MLG

The diagram of MLG construct based on pET-28a is shown in Figure 1a. MLG was overexpressed in *E. coli* BL21 (DE3) under optimal express conditions (20 °C, 0.2 mM IPTG, and induction of 36 h) and purified to homogeneity by affinity chromatography. A band at about 56 kDa in good agreement with the sum of theoretical molecular weight of M*l*QR and GDH clearly appears in Figure 1b,c, suggesting that the bi-functional enzyme MLG was successfully expressed and high purity of a target enzyme was obtained by affinity purification.

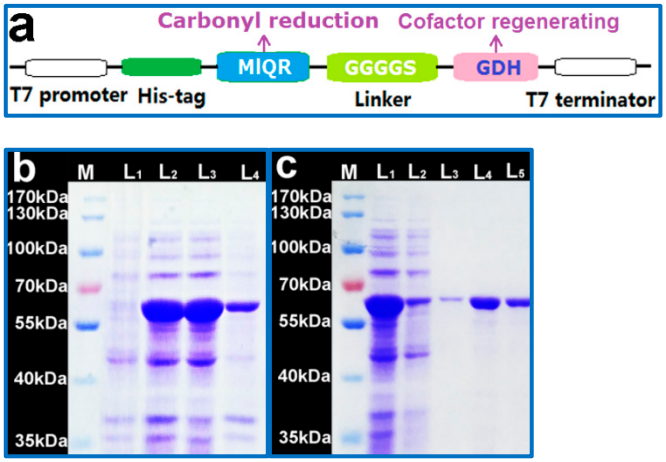

Figure 1. (**a**) Vector construct for MLG expression in T7 expression system; (**b**) MLG expression. L_M, protein molecular weight makers, L_1, and L_2, the *E. coli* BL21 (DE3) cells before and after induction, respectively. L_3 and L_4, the cell lysates and precipitate, respectively; (**c**) MLG purification. L_1, the cell lysates supernatant, L_2, flow-through; L_3, $L_{4–5}$, wash and elution fractions with 10 mM and 500 mM imidazole, respectively.

2.3. Specificity of Bi-Functional MLG to Ni@MSN Support

To test the potential advantages of Ni@MSN support to selectively and reversibly attach different kinds of His_6-tagged enzymes, the support was incubated in 1.0 mg/mL of His_6-tagged M*l*QR or GDH produced by our laboratory, respectively. Then, enzyme-loaded Ni@MSN was magnetically separated and washed with 10 mM imidazole to remove nonspecific bound enzymes, followed by eluting with 500 mM imidazole to release the bound M*l*QR or GDH. By way of comparison, the commercially Ni^{2+}-agarose bead was treated with the same amount of enzymes and same operation processes. It was found that

the Ni@MSN support exhibited much higher enzyme loading, immobilization efficiency, and purity (Figure S1a,b) than the Ni^{2+}-agarose bead (Figure S1c,d) or similar IMAC system [35], probably due to the existence of more available Ni^{2+} chelating sites in the interior pores and on the surface of the porous Ni@MSN support, which allowed more enzyme molecules to be immobilized. These results demonstrated that the Ni@MSN support could selectively and reversibly attach His_6-tagged enzymes. The amenability of Ni@MSN support to MLG was further confirmed, as evidenced by Figure 1c; an intense band corresponding to MLG presented on lanes 4–5 and impurity protein bands on the lane 2 show almost no changes in comparation with lane 1, revealing that Ni@MSN support could be served as an ideal support to selectively and efficiently enrich MLG from the cell lysates.

To enhance SEL and ELE, the immobilization conditions were optimized. The results in Figure 2a show that almost all of the MLG was adsorbed onto Ni@MSN within 0.5 h incubation and subsequent SEL did not significantly increase. Obviously, 0.5 h of incubation was sufficient to complete the MLG immobilization. As shown in Figure 2b, with the rise in temperature from 4 °C to 25 °C, ELE and SEL increased from 48.1% to 88.1% and from 28.8 to 66.8 mg/g support, respectively. However, a further increase led to a decrease in both parameters, indicating that 25 °C was preferred. Similarly, with the increase in pH from 5.0 to 8.0, both parameters increased from 41.6% to 87.3% and from 25.5 to 69.8 mg/g support, respectively. However, no significant increase was found when pH reached 10.0, demonstrating that pH 8.0 was appropriate (Figure 2c). Thus, the later immobilization experiments were carried out at pH 8.0 and 25 °C for 0.5 h of incubation. Figure 2d displayed the influence of mass ratio of support to total proteins on the immobilization. A rise in the mass ratio from 12:1 to 14:1 gave a slight increase in SEL from 70.8 to 71.7 mg/g support and an obvious increase of ELE from 85.6% to 92.7%. The mass ratios further increased from 14:1 to 17:1 and SEL decreased from 71.7 to 45.6 mg/g support, while ELE was not significantly altered. Notably, SEL of 7.17% was higher than the MOFs' [17,36] and upconversion nanoparticles [37]. Afterwards, the specific enzyme activity and activity recovery were evaluated by using 3-quinuclidinone and glucose as substrate for M*l*QR and GDH subunit in MLG, respectively. Figure 2e demonstrates that an increase in the mass ratio from 12:1 to 14:1 afforded an increase in the specific enzyme activity from 3.1 to 3.3 U/mg and 5.3 to 5.7 U/mg and the total enzyme activity recovery from 83.6% to 90.6% and 103.9% to 112.5% for M*l*QR and GDH subunit, respectively. The slightly >100% total activity recovery might be owed to the slight rise in the specific enzyme activity after immobilization. However, with a further rise in the mass ratio from 14:1 to 17:1, these parameters did not obviously change, indicating that the appropriate mass ratio was 14:1.

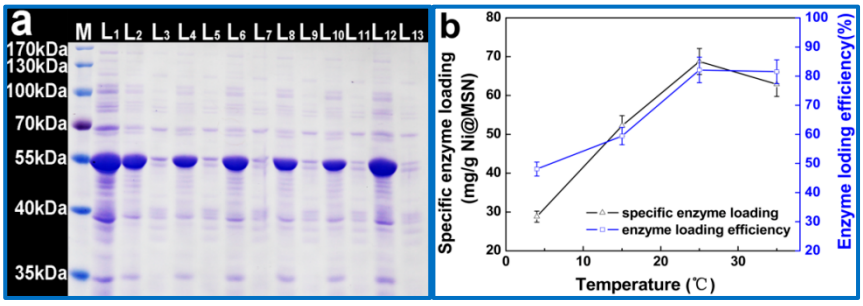

Figure 2. *Cont.*

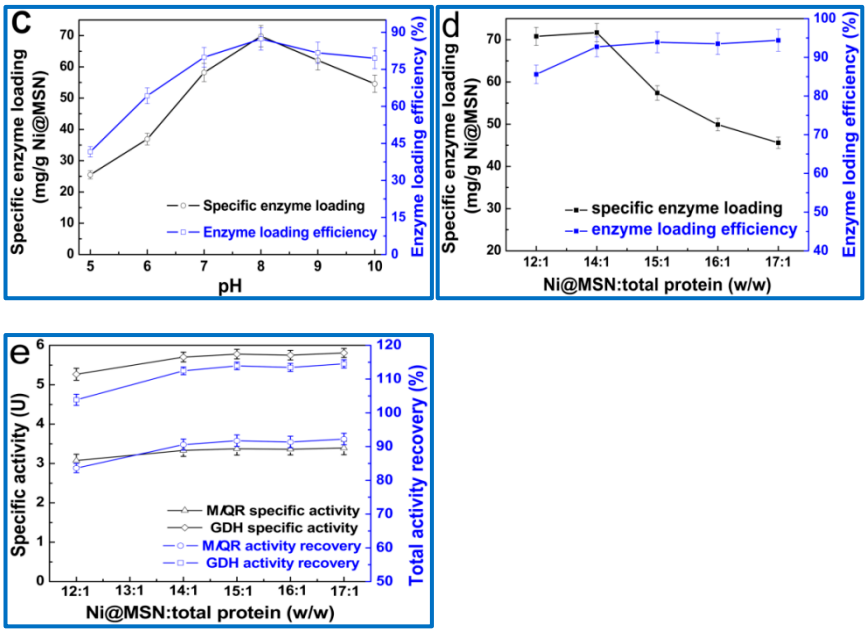

Figure 2. The influence of incubation time (**a**), temperature (**b**), pH (**c**), the mass ratio of Ni@MSN to total proteins (**d**) on the specific enzyme loading and enzyme loading efficiency, and the mass ratio of Ni@MSN to total proteins on total enzyme activity recovery and specific activity (**e**). (**a**) SDS-PAGE analysis, L_M, protein marker; L_1, the cell lysates' supernatant; $L_{2,4,6,8,10}$, and $_{12}$, the separated MLG-Ni@MSN at 0.5, 1.0, 1.5, 2.0, 2.5, and 3.0 h, respectively; $L_{3,5,7,9}$, and $_{11}$, the resultant supernatant, respectively.

2.4. Characterization of the Ni@MSN Support

The morphology and structure of Ni@MSN support and MLG-Ni@MSN were first examined by SEM and TEM. Ni@MSN exhibited a uniform, spherical shape with an average size of 20 ± 5 nm (Figure 3a–c). TEM images (Figure 3b–d) showed that the core-shell structures with a dark spot in the center of the shell (gray) were clearly seen in each particle, indicating that Fe_3O_4 nanoparticles were successfully encapsulated inside the porous silica matrix. After immobilizing MLG, the support still displayed a discrete spherical core-shell structure with an average size of 25 ± 4 nm (Figure 3e–h). It is worth mentioning that many irregular, thread-like, white stripes were clearly displayed around each particle (Figure 3f,g) compared with Figure 3b,c, and a lamellar structure was also found (Figure 3h), implying that a large amount of MLG (pointed by yellow arrows) was immobilized onto Ni@MSN.

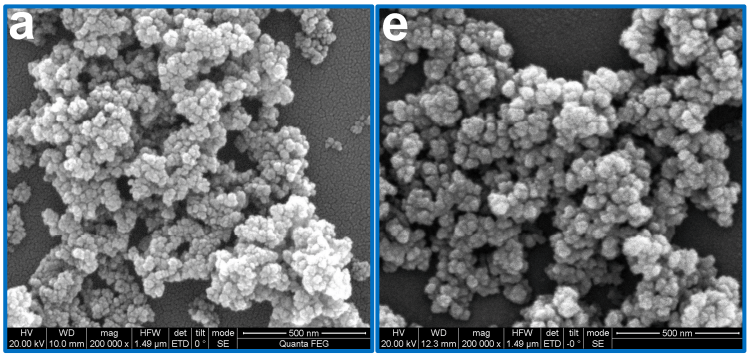

Figure 3. *Cont.*

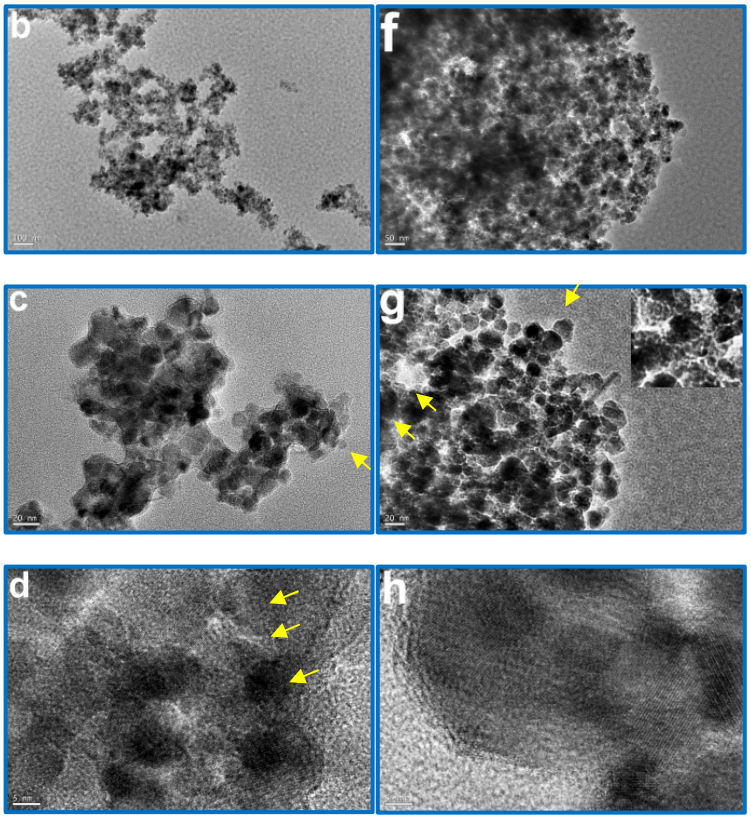

Figure 3. SEM and TEM images of Ni@MSN support (**a**–**d**) and MLG-Ni@MSN (**e**–**f**). (**c**,**d**,**g**,**h**) are TEM images of magnification of (**b**) and (**f**), respectively.

Further characterization was carried out using FTIR and XRD. Figure 4Aa shows that Fe_3O_4 gave strong characteristic peaks at 3400 cm^{-1} and 583 cm^{-1} for -OH group and Fe-O bond, respectively. The representative bands at 2957, 2925, 1700, and 1077 cm^{-1} corresponding to C-H, C=O in carboxyl group, and Si-O-Si stretching modes, respectively, along with the decrease in the intensity of -OH group (Figure 4Ab), suggested that the silylation occurred via TEOS and MPS reaction with -OH groups on the Fe_3O_4 surfaces. Note that new bands at about 1680 and 1550 cm^{-1} emerged (Figure 4Ad), which could be ascribed to the C=O stretching vibrations of amide I band and characteristic N-H bending vibrations of amide II band of MLG (Figure 4Ac). XRD was used to determine the crystal structure and its integrity. For free MLG, no crystalline peaks were found (Figure 4Bc). The diffraction peaks at 2θ = 30.26, 35.48, 43.16, 53.54, 57.12, and 62.74° (in Figure 4Ba,b,d), which corresponded to the lattice spacing of (220), (311), (400), (422),(511), and (440) planes of Fe_3O_4 crystals [38,39], respectively, matched well with the cubic inverse spinel structure of Fe_3O_4, suggesting that XRD of the as-synthesized Fe_3O_4 was in agreement with the pristine Fe_3O_4 crystal structure data (JCPDS No. 75-0033) [39]. The characteristic peak at about 23° (Figure 4Bb) was ascribed to amorphous silica [38,40], implying the formation of a core (Fe_3O_4)-shell (SiO_2) structure in Ni@MSN [38,39]. The decrease in the intensity of diffraction peaks of the Ni@MSN support and MLG-Ni@MSN was mainly because the SiO_2 shell and the immobilized MLG attenuated the incident and reflection light of X-ray. These results implied that the immobilized MLG did not aggregate into crystals.

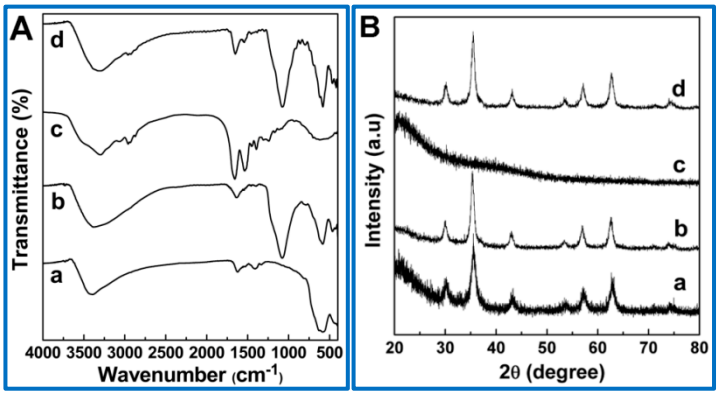

Figure 4. FTIR spectra (**A**) and XRD patterns (**B**) of Fe_3O_4 (a), Ni@MSN support (b), free MLG (c), and MLG-Ni@MSN (d).

To further verify the existence of MLG in artificial, bi-functional nanobiocatalyst, TGA was performed. The TGA curve *a* in Figure 5A shows that the sample had obvious weight loss at around 100 °C, which was attributed to the desorption of water. Curve *b* displayed a deeper drop, above 342 °C, due to the decomposition of the enzyme. According to the mass loss, the amount of the immobilized MLG was calculated to be around 7.06 wt%, in good agreement with the measured value (Figure 2d). Magnetic property was also confirmed by determining the magnetization against a function of the magnetic field strength (Figure 5B). The hysteresis loop of MLG-Ni@MSN associated with near-zero coercive force and remanent magnetism corresponded to the typical ferromagnetic characteristics [39]. The saturation magnetization of MLG-Ni@MSN (38.96 emu/g) was reduced compared with that of Fe_3O_4 (66.78 emu/g) and Ni@MSN (45.76 emu/g), which might have been caused by the SiO_2 layer coated on the Fe_3O_4 and encapsulated MLG. Even so, the saturation magnetization was sufficient, as evidenced by the fact that the biocatalyst speedily responded to an externally applied field (less than 10 s), as shown in the inset panel. After removal of the magnet, the biocatalyst could be redispersed rapidly by a gentle handshaking or ultrasound.

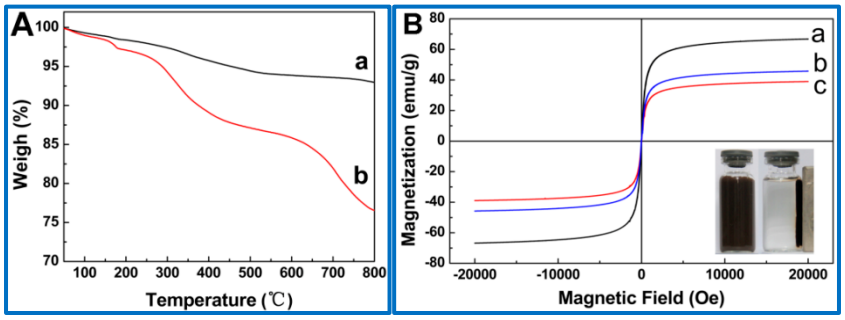

Figure 5. (**A**) TGA of Ni@MSN support (a) and MLG-Ni@MSN (b). (**B**) Magnetic hysteresis loops of Fe_3O_4 (a), Ni@MSN support (b), and MLG-Ni@MSN (c).

N_2 isotherms (Figure 6) measured at 77 K indicated that the Brunauer–Emmett–Teller (BET) surface area of Ni@MSN decreased from 70.6 to 68.1 m^2/g after association with MLG. In the range of $0.85 < P/P_0 < 1.0$, a very steep capillary condensation step was observed, indicative of a uniform and large pore size. The total pore volume and pore size of the Ni@MSN support and MLG-Ni@MSN were respectively calculated to be ~0.30 and ~0.36 cm^3/g, and 16.71 and 21.40 nm (Table S1), which were far larger than that of the reported microgel beads and could enhance the protein yields per unit mass of the carrier [41]. Notably, MLG-Ni@MSN held a larger pore size than Ni@MSN, probably because the coordination between His_6-tagged MLG and Ni^{2+} enlarged the pore size during

the embedding process [42]. Factually, such a large pore size was beneficial for the mass diffusion, making the desired nanoreactors.

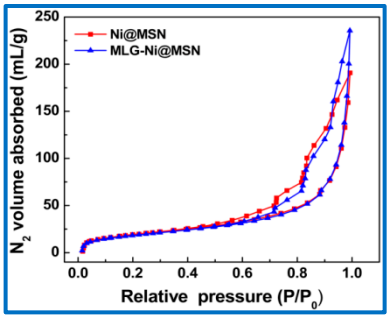

Figure 6. N_2 sorption-desorption isotherms of Ni@MSN support and MLG-Ni@MSN.

2.5. The pH and Temperature Dependence and Storage Stability

For practical applications, the artificial, bi-functional nanobiocatalyst should be stable over a wide range of pH and temperature. Thus, the effects of pH and temperature on the biocatalytic activity of free and immobilized MLG were investigated using 3-quinuclidone and glucose as substrate for M*l*QR and GDH subunit, respectively. The influence of pH dependence on the biocatalytic activity from pH 4.0 to 10.0 is shown in Figure 7a. It was observed that the maximum biocatalytic activity of the free MLG was observed at pH 7.0, while the same result was achieved at pH 8.0 for the immobilized MLG. However, the biocatalytic activity of the immobilized MLG was more than that of the free form within a wider pH range from 6.0 to 9.0, which probably benefited from the protection of the nanosystem. The influence of temperature dependence is shown in Figure 7b. As shown, the optimum temperature for the free MLG was 25 °C, whereas it was 30 °C for the immobilized MLG. However, the biocatalytic activity of the immobilized MLG increased with temperature initially, then reached a relatively stable state between 25 and 35 °C, and finally reduced slightly with further temperature elevation. In addition, much higher biocatalytic activity was still retained at a high temperature in comparison with the free form. The activities of the M*l*QR and GDH subunit in the immobilized MLG were 56.7% and 49.3%, respectively, even if the temperature rose to 50 °C, revealing that the immobilized MLG presented a high thermal stability. These results indicated that the protective networks in Ni@MSN supported retarded heat transfer and restricted active conformational changes of the entrapped MLG at higher temperature [43,44]. For biocatalyst, long-term storage stability is a prerequisite when considering its industrial applications. The differences between the residual activity of the free and immobilized MLG in the same buffer solution at 4 °C can be observed in Figure 7c, which indicated the high long-term storage stability of MLG-Ni@MSN in comparison with the free MLG. The residual activity of samples was determined at a set time interval. Remarkably, after 30 d of incubation, 85.1% and 82.0% of initial activity for M*l*QR and GDH domain in the immobilized MLG was retained, respectively, whereas the free MLG only retained 34.29% and 49.43% of the initial activity for M*l*QR and GDH domain after the same period. The improved storage stability was ascribed to the strong affinity interactions between His_6-tagged MLG with Ni^{2+}, which stabilized the active conformation of MLG, reduced enzyme leaking, and prevented the denaturation of the enzyme. Furthermore, the MLG entrapped inside the pores could be protected by the wall of pores, thus retaining higher activity in some external environments.

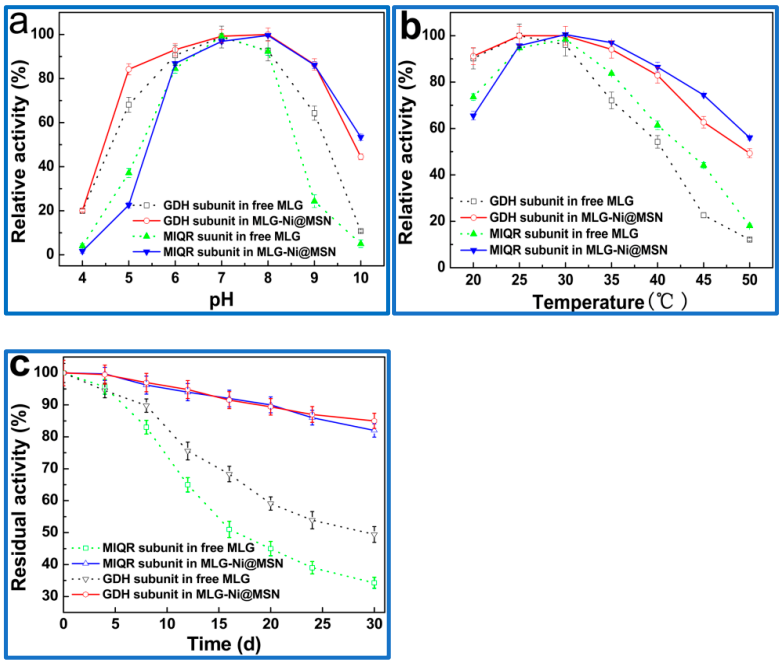

Figure 7. Effect of pH, temperature, and long-term storage period on the activity of M*l*QR and GDH subunit before and after immobilization; (**a**) pH; (**b**) temperature; (**c**) long-term storage stability.

2.6. Enzyme Kinetics

Michaelis constant (K_m) is frequently used to reflect the affinity of an enzyme to a substrate. Under optimal immobilization conditions, kinetic parameters were measured via different concentrations of glucose or 3-quinulidinone (Figure S2). The obtained parameters are listed in Table S2. Compared with free MLG, immobilization did not significantly affect either K_m or K_{cat} of GDH subunit (for glucose) in the immobilized MLG. It was found that both constants of M*l*QR subunit (for 3-quinuclidinone) were changed, but a K_m increase of about 1.5 times and a K_{cat} increase of 1.4 times led to a slight loss of K_{cat}/K_m of M*l*QR subunit activity in the immobilized MLG, mainly owing to the reduction of the conformational flexibility of M*l*QR subunit and hindering the accessibility of the substrate to the enzymes [45,46]. The V_{max} of M*l*QR subunit in the free MLG was about 1.5 times lower than its immobilized form, suggesting that the porous microenvironment facilitated the cofactor NADH derived from the GDH oxidation process diffusion to the M*l*QR active sites. These results indicated that the obtained kinetic parameters allowed the artificial, bi-functional nanobiocatalyst to be used in biotransformation of 3-quinuclidinone with cofactor regeneration.

2.7. Bioconversion

A robust biocatalyst should exhibit excellent biocatalytic performance. Bioconversion of 3-quinuclidinone by artificial, bi-functional nanobiocatalyst was investigated (Table 1). It was found that the optimum pH and temperature were 8.0 and 30 °C, respectively, and 100% conversion yield of (R)-3-quinuclidinol with >99.9% was afforded. At the same time, we also compared the biocatalytic activity of the biocatalyst at different substrate and biocatalyst loadings. Obviously, the bioconversion time obviously reduced with the increase in the amount of the biocatalyst used. Noting when the substrate loading increased from 30 to 70 g/L, 100% conversion and high selectivity (>99.9%) were still achieved. From Table 2, it can be found that the bi-functional MLG-Ni@MSN nanobiocatalyst exhibited the excellent biocatalytic performance compared with the mixture of M*l*QR and GDH or co-immobilization of M*l*QR and GDH [47] or free MLG [33]. The excellent biocatalytic performance might be ascribed to the close proximity of M*l*QR and GDH active subunit, a favored microenvironment (micropores) that maintains the conformation stability of the

immobilized MLG, and the yielded, local, high concentrations of the substrate and cofactor at the intercommunicated enzymes in the bi-functional biocatalyst. ^{1}H, ^{13}C NMR, MS, and FTIR spectra of (R)-3-quinuclidinol were in good agreement with the reported results [33]. Our findings confirmed that the bifunctional MLG-Ni@MSN biocatalyst has the potential to be applied in industrial synthesis of (R)-3-quinuclidinol.

Table 1. Asymmetric reduction of 3-quinuclidinone using bi-functional nanobiocatalyst.

Entry	Substrate (g/L)	Biocatalyst (g/L) [a]	Temperature (°C)	pH	Time (h)	Conversion (%)	ee (%)
1	50	1.0	30	8	4.0	100	>99.9
2	50	1.0	30	6	4.0	62	>99.9
3	50	1.0	30	7	4.0	94	>99.9
4	50	1.0	30	9	4.0	81	>99.9
5	50	1.0	20	8	4.0	78	>99.9
6	50	1.0	40	8	4.0	90	>99.9
7	50	1.0	50	8	4.0	67	>99.9
8	50	0.8	30	8	5.5	100	>99.9
9	50	1.2	30	8	3.5	100	>99.9
10	30	1.0	30	8	2.5	100	>99.9
11	70	1.0	30	8	6.0	100	>99.9

Reaction conditions: NAD^{+} (0.20 mM), 30 °C, PBS as reaction medium, total volume of 4 mL, pH was kept at 8.0. [a] The amount of MLG immobilized on Ni@MSN support.

Table 2. Comparison of the artificial, bi-functional nanobiocatalyst with other biocatalytic systems used for bioconversion of 3-quinuclidinone.

Entry	Biocatalyst	Loading (wt%) [a]	Actual enzyme (mg/L)	Substrate (g/L)	Time (h)	Conversion (%)	ee (%)
1	M*l*QR + GDH [b]	0.18	90.0	50	10.5	100	>99.9
2	MLG [33]	0.14	72.0	50	4.5	100	>99.9
3	Co-immobilization of QNR + GDH [47]	3.05	92.7	50	9.5	100	>99.9
4	MLG-Ni@MSN	2.0	70.6	50	4.0	100	>99.9

[a] Loading refers to the mass ratio of biocatalysts to substrate. [b] The mixture of the same amount of purified M*l*QR and GDH used as control experiment. M*l*QR and QNR mentioned in [47] are abbreviated from 3-Quinuclidinone reductases. The aim of using M*l*QR and not QNR in this study mainly was to clearly indicate that 3-Quinuclidinone reductases is from Microbacterium luteolum.

2.8. Recycling and Reusability of Bi-Functional Nanobiocatalyst

Besides the high thermal and storage stability, excellent reusability of the biocatalyst is an important merit for economic feasibility. Thus, the reusability of artificial, bi-functional nanobiocatalyst was determined to further estimate the capability of the immobilized MLG for (R)-3-quinuclidinol bioconversion. After each batch reaction, the biocatalyst was magnetically recovered, then directly applied to the next batch reaction. Figure 8a shows that the biocatalyst was able to cycle for 11 runs with 100% ee in each cycle, while the conversion yield did not significantly decrease. However, an obvious increase in the conversion time was observed for the 10th and 11th runs, implying the reduction of MLG-Ni@MSN activity. The activity loss could be ascribed to enzyme deactivation and the distortion of active sites during the separation and recycle process and the accumulation of the product on them, which hindered the active sites of the enzymes, thus affecting the next reuse. As can be seen in Figure 8b, 100% of the initial activity for M*l*QR and GDH domain were designated over three consecutive cycles, whereas their relative activity was decreased slightly after each successive cycle and was reduced to 68.3% and 65.3% after 10 consecutive cycles, and the conversion yield of (R)-3-quinuclidinol was still 100%. However, the dual-enzyme, co-immobilized MNPs' system could only retain 60% of the initial activity after six cycles [38]. The excellent reusability could mainly be attributed to the microenvironment for the enzyme encapsulated in the Ni@MSN support, which

prevented the enzyme from rapid deactivation. Notably, Figure 8c shows that the amount of the immobilized MLG did not obviously decrease after each successive cycle, indicative of negligible leaking of the enzyme during bioconversion.

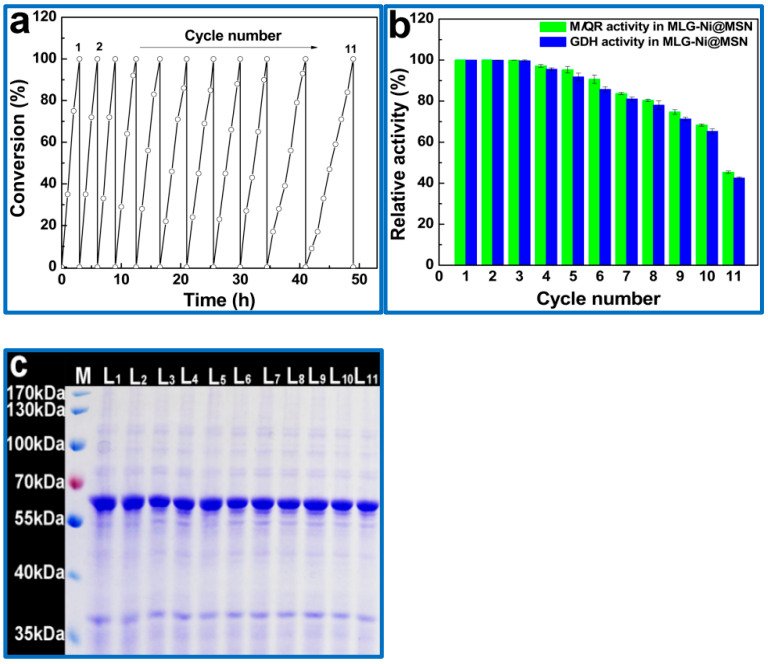

Figure 8. Recycle and reuse of the biocatalyst, (**a**) conversion yield, (**b**) relative activity of the immobilized MLG, (**c**) SDS-PAGE analysis of the change of the amount of the immobilized MLG during bioconversion, L_M, protein molecular weight marker; $L_{1–11}$, the collected biocatalyst from each cycle, respectively.

2.9. Regenerating of Ni@MSN Support

The possibility of regenerating Ni@MSN from the recovered biocatalyst after successive cycles was explored. The recovered biocatalyst was first washed using 0.5–1 M imidazole to release the bound MLG, followed by removing imidazole with EDTA. After washing with water, the MSN obtained was incubated with Ni^{2+} to regenerate Ni@MSN, followed by immobilizing MLG under the established optimal conditions, giving 68.5 mg/g and 90.7% for SEL and ELE, respectively. The specific enzyme activity and total enzyme activity recovery for M*l*QR and GDH domain were 3.1 and 5.6 U/mg and 88.9% and 99.4%, respectively. The efficient regeneration of the Ni@MSN support would significantly reduce the cost of the immobilization process and extended the practicality of MLG in industrial production.

3. Materials and Methods

3.1. Materials

Tetraethylorthosilicate (TEOS), 3-methacryloxypropyltrimethoxysilane (MPS), N,N-bis (carboxymethyl)-L-lysine, N,N-methylenebisacrylamine (MBA), isopropyl β-D-thiogalactoside (IPTG), and ammonium persulfate (AP) were from Aladdin Company (Shanghai, China). All the chemicals and reagents used were of pure analytical grade. Ni^{2+}-agarose bead (Sepharose-CL6B) was from Roche Diagnostics (Mannheim, Germany).

3.2. Synthesis of Ni@MSN Nanoparticles

3.2.1. Synthesis of MPS-Modified SiO_2@Fe_3O_4Nanoparticles

Colloidal Fe_3O_4 nanoparticles were synthesized according to the reported method [34,48]. The fresh Fe_3O_4 nanoparticles were dispersed in 150 mL water containing 4 mL $NH_3 \cdot H_2O$ under vigorous stirring at 50 °C. Then, 0.5 mL TEOS was added to the mixture. After 2 h

of the reaction, SiO_2-functionalized Fe_3O_4 nanoparticles (SiO_2@Fe_3O_4) were magnetically isolated, washed with ethanol and water, and further modified with MPS for 6 h, obtaining MPS-functionalized magnetic silica nanoparticles (MSN).

3.2.2. Synthesis of NTA-Monomer

NTA-monomer (5-acrylamido-1-carboxypentylazanediyldiaceticacid) was prepared using the reported method [41]. Briefly, 0.8 g of N,N-bis (carboxymethyl)-L-lysine was dissolved in 0.4 M ice-cooled NaOH solution. Then, 0.3 mL of the diluted acryloychloride using toluene was dripped into the mixture with constant stirring. After overnight reaction, the sample was purified by Dowex column, obtaining a thick, oil-like NTA-monomer after lyophilization.

3.2.3. Preparation of Ni@MSN Nanoparticles

Ni^{2+}-NTA-boosted, magnetic, silica nanoparticles (Ni@MSN) were synthesized by radical polymerization of MSN with NTA-monomer using MBA as the cross-linker and AP as the initiator followed by the introduction of Ni^{2+} to MSN by coordination reaction. Typically, MSN (120 mg), MBA (45 mg), and NTA-monomer (150 mg) were dispersed in 50 mL water. AP was added to initiate the polymerization reaction. After string for 6 h at 75 °C, the magnetically separated, NTA-functionalized MSN was washed with water and incubated in 1.5 M $NiCl_2$ for 2 h at 25 °C to chelate Ni^{2+}, giving Ni@MSN nanoparticles.

3.3. Synthesis of the Magnetic, Bi-Functional MLG-Ni@MSN Biocatalyst

3.3.1. Construction and Expression of Bi-Functional Enzyme MLG

The bi-functional enzyme MLG was fabricated by linking 3-quinuclidinone reductase (M*l*QR) for carbonyl reduction and glucose dehydrogenase (GDH) for cofactor regeneration via a short peptide [33]. The fusion gene *mlqr*-linker-*gdh*, namely, *mlg*, was inserted into pET-28a and then transferred into competent *E. coli* BL21 (DE3) to form the strain *E. coli* BL21 (DE3) pET28a-mlg, denoted as *E. coli* (His-MLG). *E. coli* (His-MLG) was induced to produce MLG by adding IPTG to a final concentration of 0.2 mM at 20 °C. The induced *E. coli* (His-MLG) was disrupted by XC-CD2500 Ultrasonic Oscillator (Ningbo, China), followed by centrifugation at 13,000 rpm for 10 min at 4 °C. The supernatant was filtrated by 0.22-μm filter membrane and detected by 12% SDS-PAGE. The Bradford method was used to determine enzyme concentration [49].

3.3.2. Immobilization of Bi-Functional Enzyme MLG

In this typical experiment, the desired amount of Ni@MSN support was incubated in 4 mL of enzyme solution (1.26 mg/mL) at 25 °C with shaking for 2 h. The MLG-loaded supports were magnetically separated and washed with PBS containing 10 mM imidazole to remove nonspecifically adsorbed proteins, achieving MLG-loaded Ni@MSN, denoted as MLG-Ni@MSN. To investigate the specificity of the Ni@MSN support to MLG, 500 mM of imidazole was used to elute the bound MLG. The collected samples were detected by SDS-PAGE. The effect of immobilization temperature, time, pH, and the mass ratio of the Ni@MSN support to total proteins on the enzyme activity recovery, specific enzyme loading (SEL), and enzyme-loading efficiency (ELE) were investigated. These parameters were calculated according to the following equations, respectively.

$$\text{Enzyme activity recovery } (\%) = \frac{\text{Immobilized enzyme activity (U)}}{\text{Total activity of enzyme before immobilization (U)}} \times 100 \quad (1)$$

$$\text{SEL } (\%) = \frac{\text{Immobilized enzyme (mg)}}{\text{Ni@MSN support (g)}} \times 100 \quad (2)$$

$$\text{ELE } (\%) = \frac{\text{Immobilized enzyme (mg)}}{\text{Total enzyme before immobilization (mg)}} \times 100 \quad (3)$$

Furthermore, long-term storage stability of free MLG and immobilized MLG was determined by incubating them in PBS at 4 °C without other reagents. At set intervals, the sample was withdrawn and the residual enzyme activity was analyzed based on the initial activity.

3.3.3. Determination of Enzyme Activity and Kinetic Parameters

Enzyme activity was spectrophotometrically measured at room temperature by monitoring the absorbance at 340 nm, corresponding to the change in NADH concentration by adding the 3-Quinuclidinone (10 μmol) and NADH (0.1 μmol) for M*l*QR subunit or glucose (3 μmol) and NAD^+ (0.1 μmol) for GDH subunit, and an appropriate amount of enzymes (M*l*QR or MLG-Ni@MSN) to 100 mM PBS (pH 7.0) in a total volume of 1 mL, according to the previously reported method [33]. One unit of activity (U) was defined as the amount of enzyme that catalyzed 1 μmol NADH or NAD^+ per minute. The rate of absorbance decrease or increase was proportional to the enzyme activity (U) for M*l*QR subunit reduction of 3-quinuclidinone to the corresponding (R)-3-quinuclidinol or GDH subunit oxidation of glucose to gluconate. All experiments were performed in triplicate. The enzyme activity was calculated according to the following equations, respectively.

$$\mathrm{E\ (U/mL)} = \frac{\Delta A}{\Delta t} \times V/\varepsilon \times L \times V_s \quad (4)$$

$$\varepsilon^{340}_{NADH} = 6220\ M^{-1}{\cdot}cm^{-1}$$

where $\frac{\Delta A}{\Delta t\Delta}$ is the variation value of the absorbance per minute, V is the total volume of reaction mixture, Vs is the volume of the sample, and L the light path of the cuvette (cm).

Kinetic parameters were determined by measuring the initial rates via different substrate concentration. Michaelis constant (K_m) was calculated by nonlinear regression of the Michaelis–Menten model.

3.4. Application of the Bi-Functional MLG-Ni@MSNBiocatalyst

3.4.1. Biotransformation of 3-Quinuclidone

Briefly, 60 mg of biocatalysts were added into 4 mL PBS with 3-quinuclidone (200 mg), D-glucose (300 mg), and 0.2 mM NAD^+ at 30 °C. The reaction conditions including pH, temperature, substrate concentration, and biocatalyst loading were optimized. Thin layer chromatography using CH_2Cl_2 and CH_3OH (v/v,1:9) as a developing solvent was used to monitor the reaction process. At the end of the reaction, the biocatalyst was magnetically separated and the resultant mixture was treated to collect the final product, according to the reported method [33].

3.4.2. Recycling and Regeneration of the Bi-Functional MLG-Ni@MSN Biocatalyst

In the typical reusability experiments, the first cycle was performed as follows: Biocatalyst (60 mg), 3-quinuclidinone (160 mg), D-glucose (240 mg), and 0.2 mM NAD^+ were mixed in 4 mL PBS at 30 °C. After the first cycle, the biocatalyst was magnetically recovered and directly used for a new batch reaction under the same conditions as the previous batch.

The possibility of regenerating Ni@MSN support from the recovered biocatalyst after successive reuses was also explored. The recovered biocatalyst was first washed with 1.0 M imidazole to remove the encapsulated MLG, followed by further treating with ethylenedinitrilotetraacetic acid disodium (EDTA) to release imidazole. After washing with water, the obtained MSN nanoparticles were incubated with 1.5 M $NiCl_2$ to introduce Ni^{2+}. The regenerated Ni@MSN support was directly used to immobilize MLG, using the abovementioned procedure.

3.5. Characterizations the Ni@MSN Support

X-ray diffraction (XRD) was scanned by XD-2 X-ray Diffractometer (Persee, China) with Cu K_α radiation (λ = 1.5406 Å) from 20° to 80° (2θ). Thermal gravimetric analysis

(TGA) of all samples was done from 30 to 800 °C at a heating rate of 15 °C/min under a constant flow of N_2 of 20 mL/min using Mettler 1100 SF system (Mettler, Switzerland). FT-IR was determined on Thermo Nicolet IS 50 with KBr pellets. UV-vis spectra were obtained on a Shimadazu UV-2600 spectrometer. The size and morphology of the samples were characterized by transmission electron microscope (TEM, JEOL 2100F) (Japan, Japan Electronics Co., Ltd.) and field emission scanning electron microscope (SEM, JEOL, JSM-6700F) (Japan, Japan Electronics Co., Ltd.). Samples for SEM analysis were prepared by redispersion of the collected samples in deionized water and drop-casting the solution onto freshly cleaved cover glass. Then, the glass was dried at 40 °C. Subsequently, a few-nm-thick layer of gold was sputtered onto the surface of the cover glass prior to imaging. The magnetic properties of the samples were measured by vibrating the sample magnetometer (VSM) at room temperature on a physical property measurement system DynaCool9 (Quantum, Denver, CO, USA). The surface area, pore size, and pore volume were calculated by Brunauer–Emmett–Teller (BET). The conversion yield and enantiomeric excess (ee) value were determined according the previously reported method [33,47], on a Clarus 580 GC system (Perkin Elmer, Waltham, MA, USA) equipped with a chiral capillary column (HYDRODEX-β-6-TBDM, 25 m × 0.25 mm × 0.25 μm, Macherey–Nagel) and flame-ionization detector. The injector and detector temperatures were 220 and 250 °C, respectively. The column temperature program ramped from 60 to 180 °C at 5 °C/min and was kept for 3 min by temperature-programmed methods.

4. Conclusions

In summary, we successfully employed an affinity method to simultaneously purify and immobilize MLG onto Ni@MSNto fabricate a nanosystem, which could act as an efficient biocatalyst in the conversion of 3-quinuclidinone to (R)-3-quinuclidinol with cofactor regeneration in situ with 100% conversion yield and >99% selectivity as well as a commendable reusability. Compared with free MLG, the immobilized MLG showed a broader pH and temperature tolerance and greatly improved storage stability. Importantly, the MLG-Ni@MSN biocatalyst was environmentally friendly, could be easily recovered from the reaction system, and regenerated Ni@MSN from the recovered biocatalyst. We, therefore, believe that this work opens up new opportunities for the development of a novel biocatalyst applied in a broad range of applications.

Supplementary Materials: The following are available online at https://www.mdpi.com/article/10.3390/catal11091126/s1, Figure S1: A comparison of the specificity of His6-tagged M*l*QR and GDH to different carrier. (a, b) Ni@MSN; (c, d) commercially available Ni2+-agarose bead. LM, protein molecular weight makers; L1, the cell lysates supernatant; L2, flow-through fractions, L3, L4-6, wash and elution fractions with 10 mM and 500 mM imidazole, respectively, Figure S2: The enzyme kinetics as the effect of substrate concentration on the activity of the bi-functional enzyme MLG. (a) ketoreductase (M*l*QR) in the MLG at varying glucose concentrations in the range of 0.2 to 1.0 mM, (b) cofactor regenerating enzyme (GDH) in the MLG at varying glucose concentrations in the range of 0.2 to 1.0 mM, Table S1: Porous features of Ni@MSN and MLG-Ni@MSN biocatalysts, Table S2: Kinetic parameters of the free MLG and the immobilized MLG.

Author Contributions: Conceptualization: Y.W., L.M. and Q.L.; methodology: Q.J., P.G., L.M. and Q.L.; formal analysis: Y.W. and L.M.; data curation: Y.W. and Q.L.; writing-original draft preparation: Y.W., L.M. and Q.L.; writing-review and editing: Q.L., Q.J., P.G., L.M. and Y.W. All authors have read and agreed to the published version of the manuscript.

Funding: Innovative and experimental projects of college students, Chongqing Medical University (SRIEP201960, SRIEP201974).

Data Availability Statement: Not applicable.

Conflicts of Interest: The authors declare that they have no conflict of interests.

References

1. Sharifi, M.; Sohrabi, M.J.; Hosseinali, S.H.; Hasan, A.; Kani, P.H.; Talaei, A.J.; Karim, A.; Nanakali, N.M.Q.; Salihi, A.; Aziz, F.M.; et al. Enzyme immobilization onto the nanomaterials: Application in enzyme stability and prodrug-activated cancer therapy. *Int. J. Biol. Macromol.* **2020**, *143*, 665–676. [CrossRef]
2. Balcão, V.M.; Vila, M.M. Structural and functional stabilization of protein entities: State-of-the-art. *Adv. Drug Deliv. Rev.* **2015**, *93*, 25–41. [CrossRef] [PubMed]
3. Lian, X.; Fang, Y.; Joseph, E.; Wang, Q.; Li, J.; Banerjee, S.; Lollar, C.; Wang, X.; Zhou, H.C. Enzyme-MOF (metal-organic framework) composites. *Chem. Soc. Rev.* **2017**, *46*, 3386–3401. [CrossRef]
4. Garcia-Galan, C.; Berenguer-Murcia, Á.; Fernandez-Lafuente, R.; Rodrigues, R.C. Potential of different enzyme immobilization strategies to improve enzyme performance. *Adv. Synth. Catal.* **2011**, *353*, 2885–2904. [CrossRef]
5. Benítez-Mateos, A.I.; Contente, M.L. Agarose vs. Methacrylate as Material Supports for Enzyme Immobilization and Continuous Processing. *Catalysts* **2021**, *11*, 814. [CrossRef]
6. Sheldon, R.A.; Woodley, J.M. Role of biocatalysis in sustainable chemistry. *Chem. Rev.* **2017**, *118*, 801–838. [CrossRef]
7. Thompson, M.; Penafiel, I.; Cosgrove, S.C.; Turner, N.J. Biocatalysis using immobilised enzymes in continuous flow for the synthesis of fine chemicals. *Org. Process Res. Dev.* **2019**, *23*, 9–18. [CrossRef]
8. Sheldon, R.A.; van Pelt, S. Enzyme immobilisation in biocatalysis: Why, what and how. *Chem. Soc. Rev.* **2013**, *42*, 6223–6235. [CrossRef]
9. Bilal, M.; Zhao, Y.; Tahir, R.; Hafiz, M.N.I. Magnetic nanoparticles as versatile carriers for enzymes immobilization: A review. *Int. J. Biol. Macromol.* **2018**, *120*, 2530–2544. [CrossRef]
10. Sumitra, D.; Rene, C.L.; Rajaram, Y.R.S. Enzyme immobilization an overview on techniques and support materials. *Biotechnology* **2013**, *3*, 1–9.
11. Magner, E. Immobilisation of enzymes on mesoporous silicate materials. *Chem. Soc. Rev.* **2013**, *42*, 6213–6222. [CrossRef]
12. Engström, K.; Johnston, E.V.; Verho, O.; Gustafson, K.P.J.; Shakeri, M.; Tai, C.-W.; Bäckvall, J.-E. Co-immobilization of an Enzyme and a Metal into the Compartments of Mesoporous Silica for Cooperative Tandem Catalysis: An Artificial Metalloenzyme. *Angew. Chem. Int. Ed.* **2013**, *52*, 14006–14010. [CrossRef] [PubMed]
13. Du, Y.; Gao, J.; Liu, H.; Zhou, L.; Ma, L.; He, Y.; Huang, Z.; Jiang, Y. Enzyme@ silica nanoflower@ metal-organic frame work hybrids: A novel type of integrated nanobiocatalysts with improved stability. *Nano Res.* **2018**, *11*, 4380–4389. [CrossRef]
14. Feng, D.; Liu, T.; Su, J.; Bosch, M.; Wei, Z.; Wan, W.; Yuan, D.; Chen, Y.-P.; Wang, X.; Wang, K.; et al. Stable metal-organic frameworks containing single-molecule traps for enzyme encapsulation. *Nat. Commun.* **2015**, *6*, 5979. [CrossRef] [PubMed]
15. Li, P.; Moon, S.-Y.; Guelta, M.A.; Harvey, S.P.; Hupp, J.T.; Farha, O.K. Encapsulation of a nerve agent detoxifying enzyme by a mesoporous zirconium metal–organic framework engenders thermal and long-term stability. *J. Am. Chem. Soc.* **2016**, *138*, 8052–8055. [CrossRef]
16. Chen, G.; Huang, S.; Kou, X.; Wei, S.; Huang, S.; Jiang, S.; Shen, J.; Zhu, F.; Ouyang, G.A. Convenient and versatile amino acid-boosted biomimetic strategy for nondestructive encapsulation of biomacromolecules within metal-organic framework. *Angew. Chem. Int. Ed.* **2019**, *58*, 1463–1467. [CrossRef]
17. Shieh, F.-K.; Wang, S.-C.; Yen, C.-I.; Wu, C.-C.; Dutta, S.; Chou, L.-Y.; Morabito, J.V.; Hu, P.; Hsu, M.-H.; Wu, K.C.-W.; et al. Imparting functionality to biocatalysts via embedding enzymes into nanoporous materials by a de novo approach: Size-selective sheltering of catalase in metal–organic framework microcrystals. *J. Am. Chem. Soc.* **2015**, *137*, 4276–4279. [CrossRef]
18. Cui, Y.; Li, B.; He, H.; Zhou, W.; Chen, B.; Qian, G. Metal-organic frameworks as platforms for functional materials. *Acc. Chem. Res.* **2016**, *392*, 86–95. [CrossRef] [PubMed]
19. Claudine, A.; Annie, M.; Halima, T.; Annie, M.; Jean-Louis, G.; Martine, C.S.; Wim, F.A.; Philippe, D.; André, L. Outstanding stability of immobilized recombinant α (1→3/4)-fucosyltransferases exploited in the synthesis of lewis a and lewis x tri-saccharides. *Chem. Commun.* **2000**, *20*, 2017–2018.
20. Hainfeld, J.F.; Liu, W.; Halsey, C.M.R.; Freimuth, P.; Powell, R.D. Ni-NTA-gold clusters target his-tagged proteins. *J. Struct. Biol.* **1999**, *127*, 185–198. [CrossRef]
21. Wang, W.; Wang, D.I.C.; Li, Z. Facile fabrication of recyclable and active nanobiocatalyst: Purification and immobilization of enzyme in one pot with Ni-NTA functionalized magnetic nanoparticle. *Chem. Commun.* **2011**, *47*, 8115–8117. [CrossRef]
22. Vahidi, A.K.; Yang, Y.; Ngo, T.P.N.; Li, Z. Simple and Efficient immobilization of extracellular his-tagged enzyme directly from cell culture supernatant as active and recyclable nanobiocatalyst: High-performance production of biodiesel from waste grease. *ACS Catal.* **2015**, *5*, 3157–3161. [CrossRef]
23. Vahidi, A.K.; Wang, Z.; Wong, W.S.Y.; Li, Z. Immobilization of O-acetylserine sulfhydrylase asa highly active and recyclable nanobiocatalyst:efficient synthesis of β-pyrazol-1-yl-L-alanine. *Catal. Sci. Technol.* **2016**, *6*, 6286–6293. [CrossRef]
24. Zhou, L.; Li, J.; Gao, J.; Liu, H.; Xue, S.; Ma, L.; Cao, G.; Huang, Z.; Jiang, Y. Facile oriented immobilization and purification of his-tagged organophosphohydrolase on virus-like mesoporoussilica nanoparticles for organophosphate bioremediation. *ACS Sustain. Chem. Eng.* **2018**, *6*, 13588–13598. [CrossRef]
25. Leila, T.; Tahereh, S.; Hossein, M.; Mohammad, K. Mesoporous silica nanoparticles supported copper (II) and nickel (II) schiffbase complexes: Synthesis, characterization, antibacterial activity andenzyme immobilization. *J. Solid State Chem.* **2018**, *258*, 517–525.

26. Prat, M.; Fernández, D.; Buil, M.A.; Crespo, M.I.; Casals, G.; Ferrer, M.; Tort, L.; Castro, J.; Monleón, J.M.; Gavaldà, A.; et al. Discovery of novel quaternary ammonium derivatives of (3R)-quinuclidinol esters as potent and long-acting muscarinic antagonists with potential for minimal systemic exposure after inhaled administration: Identification of (3R)-3-{[hydroxy(di-2-thienyl)acetyl]oxy-1-(3-phenoxypropyl)-1-azoniabicyclo[2.2.2]octanebrom-ide (aclidinium bromide). *J. Med. Chem.* **2009**, *52*, 5076–5092.
27. Montuschi, P.; Ciabattoni, G. Bronchodilating drugs for chronic obstructive pulmonary disease: Current status and future trends. *J. Med. Chem.* **2015**, *58*, 4131–4164. [CrossRef]
28. Naito, R.; Yonetoku, Y.; Okamoto, Y.; Toyoshima, A.; Ikeda, K.; Takeuchi, M. Synthesis and antimuscarinic properties of quinuclidin-3-yl 1,2,3,4-Tetrahydroisoquinoline-2-carboxylate derivatives as novel muscarinic receptor antagonists1. *J. Med. Chem.* **2005**, *48*, 6597–6606. [CrossRef]
29. Wang, Y.; Li, J.; Wu, Q.; Zhu, D. Microbial stereospecific reduction of 3-quinuclidinone with newly isolated nocardiasp. and rhodococcus erythropolis. *J. Mol. Catal. B Enzym.* **2013**, *88*, 14–19. [CrossRef]
30. Kolet, S.P.; Jadhav, D.D.; Priyadarshini, B.; Swarge, B.N.; Thulasiram, H.V. Fungi mediated production and practical purifi-cation of (R)-(-)-3-quinuclidinol. *Tetrahedron Lett.* **2014**, *55*, 5911–5914. [CrossRef]
31. Isotani, K.; Kurokawa, J.; Uzuki, F.S.; Nomoto, S.; Negishi, T.; Matsuda, M.; Itoh, N. Gene cloning and characterization of two NADH-dependent 3-quinuclidinone reductases from microbacteriumluteolum JCM9174. *Appl. Environ. Microbiol.* **2013**, *79*, 1378–1384. [CrossRef]
32. Zhang, W.-X.; Xu, G.-C.; Huang, L.; Pan, J.; Yu, H.-L.; Xu, J.-H. Highly efficient synthesis of (R)-3-quinuclidinol in a Space–Time Yield of 916 g L–1 d–1 using a new bacterial reductase ArQR. *Org. Lett.* **2013**, *15*, 4917–4919. [CrossRef] [PubMed]
33. Chen, Q.; Xie, B.; Zhou, L.; Sun, L.; Li, S.; Chen, Y.; Shi, S.; Li, Y.; Yu, M.; Li, W. A tailor-made self-sufficient whole-cell bio-catalyst enables scalable enantioselective synthesis of (R)-3-quinuclidinol in a high space-time yield. *Org. Process Res. Dev.* **2019**, *23*, 1813–1821. [CrossRef]
34. Chang, B.; Sha, X.; Guo, J.; Jiao, Y.; Wang, C.; Yang, W. Thermo and pH dual responsive, polymer shell coated, magnetic mesoporous silica nanoparticles for controlled drug release. *J. Mater. Chem.* **2011**, *21*, 9239–9247. [CrossRef]
35. Lee, I.S.; Lee, N.; Park, J.; Kim, B.H.; Yi, Y.W.; Kim, T.; Kim, T.K.; Lee, I.H.; Paik, S.R.; Hyeon, T. Ni/NiO Core/Shell Nano-particles for selective binding and magnetic separation of histidine-tagged proteins. *J. Am. Chem. Soc.* **2006**, *128*, 10658–10659. [CrossRef]
36. Zhang, Y.; Wang, F.; Ju, E.; Liu, Z.; Chen, Z.; Ren, X. Metal-organic-framework-based vaccine platforms for enhanced sys-temic immune and memory response. *Adv. Funct. Mater.* **2016**, *26*, 6454–6461. [CrossRef]
37. Zhou, L.; Chen, Z.; Dong, K.; Yin, M.; Ren, J.; Qu, X. DNA-mediated construction of hollow upconversion nanoparticles for protein harvesting and near-infrared light triggered release. *Adv. Mater.* **2014**, *26*, 2424–2430. [CrossRef]
38. Chen, Q.; Liu, D.; Wu, C.; Yao, K.; Li, Z.; Shi, N.; Wen, F.; Gates, I.D. Co-immobilization of cellulase and lysozyme on ami-no-functionalized magnetic nanoparticles: An activity-tunable biocatalyst for extraction of lipids from microalgae. *Bioresour. Technol.* **2018**, *263*, 317–324. [CrossRef]
39. Lee, S.; Noh JHong, S.; Kim, Y.K.; Jang, J. Dual stimuli-responsive smart fluid of graphene oxide-coated iron oxide/silica core/shell nanoparticles. *Chem. Mater.* **2016**, *28*, 2624–2633. [CrossRef]
40. Cheng, M.; Wand, Z.; Lv, Q.; Li, C.; Sun, S.; Hu, S. Preparation of amino-functionalized Fe3O4@mSiO2 core-shell magnetic nanoparticles and their application for aqueous Fe3+ removal. *J. Hazard. Mater.* **2018**, *341*, 198–206.
41. Mizrahi, B.; Irusta, S.; McKenna, M.; Stefanescu, C.; Yedidsion, L.; Myint, M.; Langer, R.; Kohane, D.S. Microgels for Efficient Protein Purification. *Adv. Mater.* **2011**, *23*, H258–H262. [CrossRef] [PubMed]
42. Hou, C.; Wang, Y.; Ding, Q.; Jiang, L.; Li, M.; Zhu, W.; Pan, D.; Zhu, H.; Liu, M. Facile synthesis of enzyme-embedded magnetic metal–organic frameworks as a reusable mimic multi-enzyme system: Mimetic peroxidase properties and colorimetric sensor. *Nanoscale* **2015**, *7*, 18770–18779. [CrossRef]
43. Kadam, A.A.; Jang, J.; Lee, D.S. Supermagnetically Tuned Halloysite Nanotubes Functionalized with Aminosilane for Covalent Laccase Immobilization. *ACS Appl. Mater. Interfaces* **2017**, *9*, 15492–15501. [CrossRef]
44. Cui, J.; Sun, B.; Lin, T.; Feng, Y.; Jia, S. Enzyme shielding by mesoporous organosilica shell on Fe3O4@silica yolk-shell nano-spheres. *Int. J. Biol. Macromol.* **2018**, *117*, 673–682. [CrossRef] [PubMed]
45. Nadar, S.; Rathod, V.K. Magnetic macromolecular cross linked enzyme aggregates (CLEAs) of glucoamylase. *Enzym. Microb. Technol.* **2016**, *83*, 78–87. [CrossRef] [PubMed]
46. Abdollahi, K.; Yazdani, F.; Panahi, R. Covalent immobilization of tyrosinase onto cyanuric chloride crosslinked amine- functionalized superparamagnetic nanoparticles: Synthesis and characterization of the recyclable nanobiocatalyst. *Int. J. Biol. Macromol.* **2017**, *94*, 396–405. [CrossRef] [PubMed]
47. Yu, M.; Liu, D.; Sun, L.; Li, J.; Chen, Q.; Pan, L.; Shang, J.; Zhang, S.; Li, W. Facile fabrication of 3D porous hybrid sphere by co-immobilization of multi-enzyme directly from cell lysates as an efficient and recyclable biocatalyst for asymmetric reduction with coenzyme regeneration in situ. *Int. J. Biol. Macromol.* **2017**, *103*, 424–434. [CrossRef]
48. Yue, Q.; Zhang, Y.; Jiang, Y.; Li, J.; Zhang, H.; Yu, C.; Elzatahry, A.A.; Alghamdi, A.; Deng, Y.; Zhao, D. Nanoengineering of core–shell magnetic mesoporous microspheres with tunable surface roughness. *J. Am. Chem. Soc.* **2017**, *139*, 4954–4961. [CrossRef] [PubMed]
49. Bradford, M.M. A Rapid and sensitive method for the quantitation of microgram quantities of protein utilizing the principle of protein-dye binding. *Anal. Biochem.* **1976**, *72*, 248–254. [CrossRef]